JGR Earth Surface

RESEARCH ARTICLE
10.1029/2021JF006071

An Ecogeomorphic Framework Coupling Sediment Modeling With Invasive Riparian Vegetation Dynamics

Jordan T. Gilbert[1] and **Andrew C. Wilcox**[1]

[1]Department of Geosciences, University of Montana, Missoula, MT, USA

Key Points:

- Basin-scale ecogeomorphic models provide insights into physical and ecological dynamics of fluvial systems and can guide management
- Invasive species such as *Arundo donax*, which is modeled here, alter ecogeomorphic feedbacks and are influenced by sediment balances
- Coupling a vegetation recruitment model with a model of sediment balances and floodplain erosion highlighted invasive-plant source areas

Correspondence to:
J. T. Gilbert,
jordan1.gilbert@umontana.edu

Citation:
Gilbert, J. T., & Wilcox, A. C. (2021). An ecogeomorphic framework coupling sediment modeling with invasive riparian vegetation dynamics. *Journal of Geophysical Research: Earth Surface*, *126*, e2021JF006071. https://doi.org/10.1029/2021JF006071

Received 7 JAN 2021
Accepted 3 JUN 2021

Abstract Feedbacks between geomorphic processes and riparian vegetation in river systems are an important control on fluvial morphodynamics and on vegetation composition and distribution. Invasion by nonnative riparian species alters these feedbacks and drives management and restoration along many rivers, highlighting a need for ecogeomorphic models to assist with understanding feedbacks between plants and fluvial processes, and with restoration planning. In this study, we coupled a network-scale sediment model (Sediment Routing and Floodplain Exchange; SeRFE) that simulates bank erosion and sediment transport in a spatially explicit manner with a recruitment potential analysis for a species of riparian vegetation (*Arundo donax*) that has invaded river systems and wetlands in Mediterranean climates worldwide. We used the resulting ecogeomorphic framework to understand both network-scale sediment balances and the spread and recruitment of *A. donax* in the Santa Clara River watershed of Southern California. In the coupled model, we simulated a 1-year time period during which a 5-year recurrence interval flood occurred in the mainstem Santa Clara River. Outputs identify key areas acting as sources of *A. donax* rhizomes, which are subsequently transported by flood flows and deposited in reaches downstream. These results were validated in three study reaches, where we assessed postflood geomorphic and vegetation changes. The analysis demonstrates how a coupled model approach is able to highlight basin-scale ecogeomorphic dynamics in a manner that is useful for restoration planning and prioritization and can be adapted to analogous ecogeomorphic questions in other watersheds.

Plain Language Summary The interactions between river flows and plants control how the physical river environment and the river's plant communities respond to floods and change through time. For this reason, vegetation models coupled with sediment models can help to advance understanding of river systems. Invasive vegetation is common in rivers throughout the world, and can change these interactions. In this study, we combined a vegetation model and a sediment model to understand the spread of an invasive plant, *Arundo donax*, in the Santa Clara River watershed of Southern California. By doing so, we found that particular river reaches act as a source of invasive plants that can then move downstream and reestablish lower in the watershed. This approach demonstrates the usefulness of these coupled models for answering questions about river systems and for planning restoration and management actions.

1. Introduction

Bidirectional interactions between riparian vegetation and fluvial processes are important drivers of the physical and ecological development of river-floodplain ecosystems (Corenblit et al., 2007; Osterkamp & Hupp, 2010). Sediment transport and deposition create patches conducive to recruitment of pioneer riparian vegetation (Fraaije et al., 2015; Gurnell et al., 2012) and can also cause vegetation mortality through bed scour, bank erosion, or burial (Bywater-Reyes et al., 2015 Kui & Stella, 2016). Riparian vegetation, in turn, creates heterogeneity in flow velocity fields and resulting sediment transport capacity (Manners et al., 2013, 2015) and stabilizes bars and banks, influencing planform and geometry (Gran & Paola, 2001; Tal & Paola, 2010). Fluvial processes produce a disturbance gradient that can promote or inhibit recruitment of particular vegetation guilds, which are assemblages of functionally similar plants (Fraaije et al., 2015; Hough-Snee et al., 2015; Merritt et al., 2010) with traits that produce distinct plant-morphodynamic interactions (Diehl, Merritt, et al., 2017; Diehl, Wilcox, et al., 2017). Because of these interactions, changes in the composition of riparian species and associated traits, as are caused by nonnative species invasions, have important implications for channel form and overall ecosystem structure and function. Nonnative riparian

Figure 1. Aerial (a) and ground (b) views of a dense, monotypic arundo stand in a floodplain riparian area, Santa Clara River, CA.

species are a common stressor of river-floodplain ecosystems globally (Friedman et al., 2005; Hardion et al., 2014; Richardson et al., 2007) and often differ from native species both ecologically and morphologically. As a result nonnative species have distinct effects on channel roughness, flow velocities, bank stability, erosion and deposition, and channel morphology (Cadol et al., 2011; Martinez & McDowell, 2016; McShane et al., 2015; Rowntree, 1991; Van Oorschot et al., 2017).

Arundo donax (commonly known as giant reed, hereafter arundo) is a prominent invasive species that drives changes to physical and ecological processes in river-floodplain systems and in turn motivates management and restoration concerns. Arundo is a perennial, large-statured grass that is native to tropical and temperate regions of the greater Middle East, and it has invaded riparian corridors and wetlands in Mediterranean climates worldwide (Hardion et al., 2014). Arundo frequently grows in dense, monotypic stands (Lambert et al., 2010) (Figure 1) in a manner that can have cascading effects on community vegetation assemblages, displacing native vegetation and altering riparian and aquatic habitat (Cushman & Gaffney, 2010; Maceda-Veiga et al., 2016). Arundo invasions have likely been facilitated by adaptations that make it well suited to thrive within the natural and anthropogenic disturbance regimes common in Mediterranean climates (Quinn & Holt, 2008). For example, arundo is adapted to wildfire: it provides excellent fuel, especially in late autumn and winter when it dries and dies back, thus increasing landscape susceptibility to fire, and it rapidly colonizes and grows quickly following fire (Coffman et al., 2010). Arundo grows in a variety of soils and soil moisture conditions, but thrives in mesic soils of floodplains (Quinn & Holt, 2008). Increased availability of nitrogen and other nutrients (Coffman, 2007; Lambert et al., 2014), as often occurs in runoff associated with urban and agricultural land use, also creates conditions favorable for arundo establishment.

Interactions between fluvial sediment dynamics and arundo are poorly understood but potentially important both for channel form and processes, and for arundo spread and recruitment. Outside of its native range, arundo seeds are sterile, and the plant reproduces vegetatively via rhizomes (Saltonstall et al., 2010). High flows uproot and transport arundo plants, breaking off portions of rhizomes that, when subsequently deposited in fresh, bare sediments rapidly take root and establish (Lambert et al., 2014). Rhizome fragments as small as 2 cm^2 will sprout in a variety of soil types, depths and soil moisture conditions (Boose & Holt, 1999; Wijte et al., 2005). Because of this dependence on rhizome transport for reproduction, arundo invasion spreads from upstream to downstream in watersheds (Bell, 1998).

Arundo establishes well in depositional environments with high water availability, such as riparian zones. Arundo has a lower tensile strength than most riparian species native to Mediterranean climates, and has shallow rooting depths compared with many of these plants (Stover et al., 2018). These factors result in reduced bank stability where arundo establishes compared to banks colonized by native vegetation (Stover et al., 2018), potentially facilitating channel change and additional uprooting and transport of arundo plants. Consequently, bank erosion and sediment transport are important components in understanding and modeling interactions between fluvial processes and this riparian species.

Despite advances in understanding of vegetation-morphodynamic feedbacks (e.g., Politti et al., 2018), vegetation is poorly, and often only implicitly, represented in models of sediment dynamics at various scales. Coupled with representations of vegetation dynamics, sediment models can facilitate understanding and prediction of morphologic evolution, changes to vegetation composition and cover, and their interactions. Most sediment models that explicitly account for lateral interaction with the floodplain are applied at localized (reach) scales rather than at the larger (catchment) scale pertinent to management problems such as riparian invasions or land use change. Both conceptual (e.g., Corenblit et al., 2007) and numerical (Caponi et al., 2020; Solari et al., 2016) models linking plants and morphodynamics have been developed to highlight different components of these relationships, including the effect of vegetation on river meandering and planform (e.g., Crosato & Saleh, 2011; Perucca et al., 2007), and on flow and sediment dynamics (e.g., Bertoldi et al., 2014; Camporeale et al., 2013; Hooke et al., 2005; Shields et al., 2017).

Sediment models focused on bank erosion and channel stability conceptualize the relevant cohesive and erosive forces, including the effects of vegetation, differently at different spatial scales. The cohesive forces are determined by soil characteristics such as clay content (Couper, 2003), pore-water pressure in the soil, and density and configuration of roots (Millar, 2000; Pollen-Bankhead & Simon, 2010). Additionally, some models account for decreased erosional effectiveness due to bank-strengthening feedbacks such as slump-block failure creating bank armor (Parker, Shimizu, et al., 2011). Erosional forces causing bank erosion can be characterized at coarse scales using metrics like reach-averaged or excess shear stress (Partheniades, 1965) or stream power, or at fine scales based on the velocity structure of the flow (Parker, Shimizu, et al., 2011; Pizzuto & Meckelnburg, 1989). Morphodynamic models assess bank erosion by coupling bank-stability and geotechnical-failure models (e.g., Darby et al., 2007; Klavon et al., 2017; Simon et al., 2000). At broader scales, where such models are difficult to parameterize, characteristics such as channel radius of curvature (or sinuosity), valley confinement, cumulative stream power, and surrounding land use have been shown to correlate with bank erosion (Janes et al., 2017; Larsen et al., 2006; Micheli et al., 2004).

Coupled models of vegetation and sediment dynamics that incorporate floodplain interactions and feedbacks between flow, sediment transport, and vegetation recruitment and mortality not only facilitate assessment of relationships between the physical processes and riparian vegetation dynamics of river systems, but can also inform riparian management and restoration decision making. In this study, we present an ecogeomorphic framework combining sediment and riparian vegetation models. Specifically, we combined a catchment-scale, spatially explicit model of sediment dynamics with a simple recruitment model for an invasive riparian species, *Arundo donax*. We applied this analysis to the Santa Clara River basin in Southern California, where arundo invasion is a key concern for river and floodplain management in a landscape influenced by agriculture, dams, urbanization, and wildfire. Our objectives are to (a) demonstrate an approach to combining sediment and vegetation dynamics into a coupled ecogeomorphic framework; (b) use this modeling to provide insights into interactions between physical and ecological processes; and (c) illustrate applicability to a specific river system and invasive species and to management and restoration.

2. Methods

2.1. Study Area

Arundo has invaded rivers across Southern California, displacing native willow and cottonwood, and consequently reducing habitat quality for native aquatic and riparian species, as well as increasing channel roughness and altering morphodynamics. In this study, we focus specifically on the sediment dynamics and arundo invasion of the Santa Clara River watershed (Figure 2). The Santa Clara River drains one of the largest coastal basins in Southern California (~4,200 km^2). The river begins in the San Gabriel Mountains of the Western Transverse Ranges, and flows west for ~135 km to where it drains into the Pacific Ocean. The mountainous areas in the lower basin receive 100 cm of rain annually, compared to the 20 cm that the valley of the upper basin receives. Temperatures are also much more variable in the upper basin (average monthly high range = 17.6°C–34.9°C) than at the basin outlet (19°C–23°C). Overall, the basin has a Mediterranean climate; most precipitation falls during winter and spring months, and summer and autumn months are generally warm and dry. Infrequent, high-intensity, short-duration storms produce the majority of the precipitation, resulting runoff (Andrews et al., 2004), and geomorphic work within the watershed (Williams, 1979). Multiyear droughts, such as from 2012 to early 2017, influence groundwater conditions, vegetation distribution, and ecogeomorphic processes. The combination of erodible (sedimentary) rock in most lower-elevation portions of the basin and large uplift rates result in high sediment production (~2,000 tonnes km^{-2} yr^{-1}) (Booth et al., 2014; Orme, 1999; Warrick & Mertes, 2009).

Despite its proximity to the Los Angeles metropolitan area, the anthropogenic imprint on the Santa Clara River is in some respects modest, and it remains the longest free-flowing river in southern California. Much of the catchment's land, especially in upland areas, is publicly owned including designated wilderness. The Santa Clara River's valley along the mainstem has largely been converted to agriculture, but some floodplains remain laterally connected to the river. Urbanization is concentrated near the river's mouth in Ventura and the Oxnard plain, and in the Santa Clarita Valley on the upper river. A history of disturbance dating to European settlement in the 1800s, however, has altered flow and sediment dynamics within the watershed, as summarized by Downs et al. (2013). In the mid-1900s, several large dams were constructed

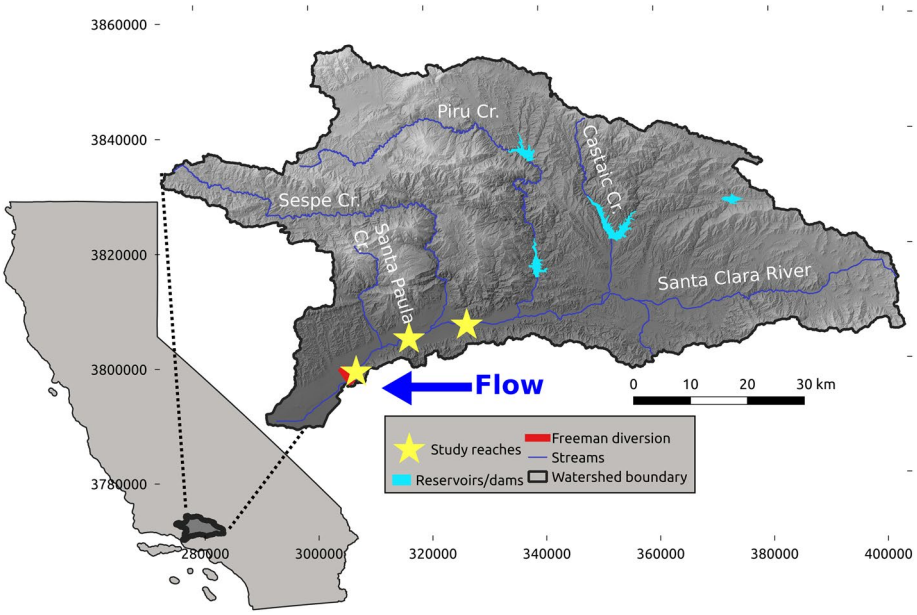

Figure 2. Location of the Santa Clara River watershed in Southern California, including validation (study) reach locations. The river drains into the Pacific Ocean at Ventura, CA. Coordinates in this (bottom and left side of map) and all subsequent figures are in the NAD 83 UTM Zone 11N projected coordinate reference system.

on tributaries (Figure 2), and the Santa Clara River corridor was also impacted by levees and bank armoring for flood control, and aggregate mining. In the lower river, mining caused significant incision, creating a knickpoint that migrated upstream and prompted construction of the Vern Freeman Diversion (Figure 2) in 1991, for grade control and to recharge depleted groundwater. Wildfires, which generally occur from late summer through autumn, are an important component of the basin's disturbance and sediment regime (Florsheim et al., 1991; Keeley & Fotheringham, 2001; Warrick & Rubin, 2007). Finally, arundo invasion has been a longstanding and ongoing disturbance along the river (e.g., Figure 1). Arundo was intentionally planted in the area as long ago as the early 1820s for erosion control and as a windbreak (Dudley, 2000). Since then hydrology and agricultural practices (e.g., changes in cattle grazing, nutrients) have influenced arundo distribution. The flood of record (1969) redistributed arundo widely throughout floodplains and terraces along the river. Large, persistent stands from this event remain, and subsequent flood events have further redistributed arundo through the mainstem Santa Clara River.

The Santa Clara River corridor provides important habitat to endangered species of songbirds, including the Southwestern Willow Flycatcher (*Empidonax traillii extimus*) and Least Bell's Vireo (*Vireo bellii pusillus*) (Stanton et al., 2019), and supports the southernmost population of Steelhead trout (*Oncorhynchus mykiss*), whose populations have plummeted as a result of disturbances to the river system (Kelley, 2004). Restoration planning and implementation have ranged from restoring connectivity by upgrading or removing diversions, culverts, and other obstacles to fish passage, to ecological restoration of riparian areas by removing arundo and replanting native vegetation to benefit bird species (Kus, 1998). For example, The Nature Conservancy has purchased land parcels along the river as conservation nodes to increase connectivity for wildlife and as sites for active riparian-ecosystem restoration (Parker et al., 2014, 2016).

2.2. Modeling and Analysis

To address our objective of demonstrating an approach to combining sediment and vegetation dynamics into a coupled ecogeomorphic framework, we linked (a) a simple statistical model of arundo recruitment potential that we developed using geospatial analyses of remote sensing data, and (b) a spatially explicit model of basin sediment dynamics, which was calibrated and validated using field data that we collected in addition to previously collected datasets. For geospatial analysis and modeling purposes, we used a shapefile of the Santa Clara River and some of its major tributaries. This shapefile was broken into reaches of

~1 km in length (ranging from 0.515 to 2 km). Here, we focus on 90.8 km of the mainstem river from its mouth to 15.3 km upstream of Castaic Creek (Figure 2).

2.2.1. Sediment Modeling

To model basin sediment dynamics, we used the Sediment Routing and Floodplain Exchange (SeRFE) model (Gilbert & Wilcox, 2020). SeRFE is a spatially explicit, geospatial model that simulates sediment recruitment, transport, and deposition on a reach-by-reach basis at the scale of an entire basin. It uses floodplain delineation and channel confinement algorithms to quantify sediment storage in floodplains, and the proportion of the network that can laterally adjust through bank erosion to recruit floodplain sediment. SeRFE uses a generalizable, excess stream power bank-erosion equation that is calibrated to the basin based on measurements of bank erosion. Disturbances that alter sediment and flow regimes, such as dams, wildfires, and landslides can be accounted for in SeRFE simulations. Here, we present the elements of SeRFE essential to its use in our ecogeomorphic framework for linking sediment and invasive-plant dynamics. Additional details on SeRFE are presented in Gilbert and Wilcox (2020).

SeRFE calculates rates of sediment transport and bank erosion based on excess stream power. Stream power is defined as the rate of energy dissipation of the flow against the channel bed and banks, and is calculated by

$$\Omega = \rho g Q S \tag{1}$$

where Ω is total stream power (W m^{-1}), ρ is the density of water (kg m^{-3}), g is acceleration due to gravity (m s^{-2}), Q is discharge (m^3 s^{-1}), and S is bed slope (dimensionless). Dividing Ω by channel width results in unit stream power (ω). To calculate sediment transport, SeRFE uses an empirical equation (Lammers & Bledsoe, 2018):

$$q_s = 0.0214\left(\omega_0 - \omega_{c\,\mathrm{bed}}\right)^{\frac{3}{2}} D^{-1} q^{-\frac{5}{6}} \tag{2}$$

where q_s is sediment flux (ppm), ω_0 is reach-averaged unit stream power, $\omega_{c\ \mathrm{bed}}$ is the critical unit stream power at which bed-material motion begins, D is a representative bed grain diameter (m), and q is unit discharge (Q divided by channel width). Bank erosion is calculated using

$$\varepsilon = k\left(\omega_0 - \omega_{c\,\mathrm{bank}}\right)^{a} \tag{3}$$

where erosion rate ε is in m s^{-1}, k is an erodibility parameter (m^3 W^{-1}), $\omega_{c\,\mathrm{bank}}$ is the critical unit stream power at which bank erosion begins, and a is a dimensionless exponent, here set to 0.5 (after Khanal et al., 2016), that scales the relationship between bank erosion rate and excess stream power.

The model was calibrated using routines that attribute each network segment with values for the variables in Equations 2 and 3, such that the sediment transport and bank erosion equations can be applied to every segment of the input drainage network. As sediment transport is highly dependent on bed grain size (D), SeRFE uses an extrapolation algorithm based on modeled hydraulics to model median grain size and a prediction range for every reach of the drainage network using grain-size data. In this application, we used grain-size data collected by the USGS and Stillwater Sciences (2011).

Grain size estimates can then be used to calculate $\omega_{c\,\mathrm{bed}}$ based on Parker, Clifford et al., (2011)'s relation for dimensionless stream power (ω_{c*}):

$$\omega_{c*} = \frac{\omega_{c\,\mathrm{bed}}}{g\left(\rho_s - \rho\right)\sqrt{\frac{\rho_s - \rho}{p} g D^3}} \tag{4}$$

where ρ_s is the density of sediment (kg m^{-3}). Various incipient motion datasets suggest an average ω_{c^*} of 0.1 (Lammers & Bledsoe, 2018; Parker, Clifford et al., 2011), which we combined with the modeled values of D to find $\omega_{c\,\mathrm{bed}}$.

Next, we used our estimates of bed mobilization thresholds ($\omega_{c\,\mathrm{bed}}$) to model bank erosion. We link $\omega_{c\,\mathrm{bank}}$ and $\omega_{c\,\mathrm{bed}}$ using a bank mobilization factor (Θ), which scales the stream power required to mobilize the banks compared to the bed:

$$\omega_{c\,\mathrm{bank}} = \theta * \omega_{c\,\mathrm{bed}} \tag{5}$$

Equation 5 relies on the assumption that $\omega_{c\,\mathrm{bank}}$ varies linearly with $\omega_{c\,\mathrm{bed}}$ and is similar to the μ' metric used by Millar (2005). When $\Theta = 1$, bed mobilization and bank erosion initiate at the same flow, and $\Theta > 1$ means that additional stream power is required to initiate bank erosion. For the Santa Clara River basin, where channels are mostly labile, with mixed sand and gravel beds and incipient bed motion expected to begin well below bankfull, we obtained an average Θ value of 4.2 to use in the modeling (Gilbert & Wilcox, 2020). With Θ parameterized, bank erosion can be modeled using Equation 3. Soil erodibility (k) can be calibrated by adjusting its value and applying Equation 3 using flow records associated with the reach, until error between measured bank erosion, which we determined from comparing digital elevation models (DEMs) from two different dates, and modeled bank erosion is minimized. With all of the necessary variables in Equations 2 and 3 thus parameterized, the SeRFE model can be applied to each reach of the input stream network for the duration of the flow record provided. For more detail on this calibration and discussion of limitations of this approach, see Gilbert and Wilcox (2020)

SeRFE tracks flow, sediment flux, sediment storage, and sediment balance outputs for each network reach at each time step. Sediment storage can be separated into channel and floodplain components All outputs can be visualized or summarized over a specified time interval. For the application presented here, we ran SeRFE using the hydrograph for the 2017 water year, during which a moderate (~5-year recurrence-interval) flood occurred. We associated the primary, low-flow channel with channel sediment storage and any secondary channels, as well as floodplains, with floodplain sediment storage. We focus on the sediment balance output and the floodplain sediment storage outputs due to their importance with respect to arundo transport and recruitment during the hydrologically active period of the simulation (days 232–295; there was little to no flow during the remainder of the time period simulated). Sediment balance is represented in SeRFE outputs using a "Capacity to Supply Ratio" (CSR) which is simply the transport capacity for each reach divided by the sediment available for transport (Soar & Thorne, 2001). Sediment fluxes and storage are in tonnes, using an assumed bulk density for the basin to convert from volume to mass.

2.2.2. Arundo Mapping and Recruitment Potential Analysis

We used Google Earth imagery from summer 2018 to map arundo stands. Because of its unique spectral and textural signatures, arundo is readily identifiable in aerial imagery (Fernandes et al., 2013). For the previously mentioned 90.8 km of the Santa Clara River, we delineated stands, which we defined as groups of vegetation in which arundo comprised 50% or more of the areal extent, at a ~1:3,000 scale. Arundo stands were previously mapped as well (Stillwater Sciences & URS Corporation, 2007), allowing comparison of arundo distribution in the intervening decade.

We categorized each reach of the river according to arundo recruitment potential based on two criteria: groundwater availability/base flow regime and potential floodplain nutrient enrichment (Decruyenaere & Holt, 2005; Lambert et al., 2014). To determine the first of these, we characterized the flow regime of each reach as quasiperennial, intermittent, or dry. There are six distinct groundwater basins along the lower river, with varying depths and degree of interaction with the surface. Two narrows, Piru Narrows, and Fillmore Narrows, occur where groundwater reservoirs are restricted by faulting, causing upwelling of groundwater (Burton et al., 2011). We classified river reaches where upwelling groundwater results in surface-water flow for six or more months of the year as quasi-perennial. Reaches that are underlain by groundwater that fills during the rainy months, creating saturated conditions that result in dependable intermittent flow during the wet season (fewer than six months) were classified as intermittent. In the remainder of the reaches, groundwater basins are much deeper, resulting in losing reaches that only flow during floods. We classified these reaches as dry.

Table 1
Rule Table for the Arundo donax Source/Sink Analysis

Arundo recruitment potential	Predicted topographic change[a]	Confidence in topographic change[b]	Arundo zone type
High	Erosion	High	Strong source
High	Erosion	Moderate	Moderate source
High	Deposition	High	Strong sink
High	Deposition	Moderate	Moderate sink
High	None		None
Moderate	Erosion	High	Moderate source
Moderate	Erosion	Moderate	Weak source
Moderate	Deposition	High	Moderate sink
Moderate	Deposition	Moderate	Weak sink
Moderate	None		None
Low			None

[a]as modeled by SeRFE for 5-year recurrence interval flood. [b]based on the range of uncertainty in the model outputs.

Because nutrients facilitate arundo invasion, we then identified reaches where floodplain soils potentially have higher nutrient content due to agricultural practices. To do so, we identified canals that drain agricultural lands, terminating in the river corridor. We used the National Land Cover Data set (NLCD), a 30-m resolution LANDSAT-derived data set to delineate agricultural lands along the river, and extracted flow lines encoded as canals from the United States Geologic Survey's (USGS) National Hydrography Datasets (NHD). Each reach of the drainage network was then classified as intersecting canals or not.

To develop a model for arundo recruitment, we determined arundo presence for each reach, as well as the stand area when present. The floodplain was split using a Thiessen polygon algorithm, which generates polygons, each of which is intersected by a single stream reach, and within which every point is nearer to that reach's midpoint than to any other reach's midpoint, and we calculated the arundo stand area within each polygon. Next, we developed a logistic regression model for predicting the probability of the presence of arundo from the categorical input values assigned to each reach. The model was trained using 70% of the reaches, and tested on the remaining 30%. After parameterizing the logistic model, reaches were then given a categorical recruitment potential class based on predicted probability of arundo presence (low: <25%; moderate: 25%–75%; high: >75%). We then used the Kruskal-Wallis test to determine whether the median of the distribution of stand area was different for each of the recruitment potential classes. This nonparametric test was suitable because more than two classes were compared, and the stand-area data for all classes was skewed, with large numbers of zero values in reaches where no stands occurred.

2.2.3. Arundo Sources and Sinks

To produce a coupled ecogeomorphic framework relating sediment dynamics and arundo recruitment, we combined the outputs of the arundo recruitment potential analysis with the floodplain erosion/deposition outputs from SeRFE, producing an output highlighting potential source and sink zones for arundo. We used a simple inference system with a rule table (Table 1) to characterize zones as strong, moderate, or weak sources or sinks for arundo. Reaches were assigned a categorical value for confidence in floodplain erosion or deposition based on the modeled range of floodplain change for the reach, which accounts for uncertainty based on uncertainty in median bed grain size. Because this uncertainty propagation results in broad confidence intervals, the range often spans both positive and negative values. Therefore, in cases where the entire range of modeled floodplain topographic change was positive or negative, we assigned high confidence of deposition or erosion, respectively. If the majority (i.e., >50%) of the range was positive or negative, we assigned moderate confidence of deposition or erosion. While the recruitment model incorporates some basic ecological elements of arundo spread and recruitment, this coupled model focuses on the geomorphic drivers of arundo dynamics. Other ecological processes that may be important in arundo dynamics are not explicitly modeled in this framework (see Discussion).

2.3. Model Output Validation

We assessed model outputs in three validation reaches (length ~500 m) where we performed photogrammetric UAV surveys in summer 2018 to generate aerial orthophotos and structure from motion (SfM) DEMs. In the three reaches, restoration actions targeted at reducing arundo coverage are in various stages of planning and implementation. The upper validation reach is above the confluence of Sespe Creek with the Santa Clara River, the middle reach is between Sespe and Santa Paula creeks, and the lower reach is below Santa Paula Creek, just upstream of the Vern Freeman Diversion (Figure 2).

To validate our Google Earth imagery classification, and to assess temporal change in arundo area, we used aerial imagery collected during the photogrammetric surveys. We classified orthophotos of each reach into

eight ground cover classes using a maximum likelihood supervised classification algorithm in ArcGIS. We then extracted the pixels classified as arundo, and we used a DBSCAN clustering algorithm to group arundo pixels into stands. Stands were defined as clusters of at least 100 pixels (10 m^2), where distances between pixels were no more than 8 m. These clusters were then polygonized to compare to a previous classification from 2007. Polygons in the 2007 data set characterized as having 50% or greater arundo cover were extracted to maintain the same "stand" definition throughout all datasets.

Last, we assessed geomorphic change at the validation reaches by comparing lidar DEMs from 2015, which was the most recent data set prior to the flood, and DEMs for 2018 that we generated using SfM, as well as imagery from both dates. DEMs were used to quantify planform change, and imagery was used to identify floodplain deposition and erosion, as well as changes in arundo distribution. We compared these estimates of geomorphic change with SeRFE model outputs. In the middle reach, we further validated simulated geomorphic change by performing hydraulic modeling simulations using FaSTMECH, a quasisteady multidimensional flow model within iRIC (Nelson et al., 2016). FaSTMECH simulations were applied to flows approaching the 2017 peak flow and used the 2015 lidar DEM for topography. This allowed us to assess the patterns of floodplain inundation and resulting deposition at a finer spatial resolution and compare it to the reach-level results from SeRFE.

3. Results

3.1. Sediment Modeling

Sediment balance, as modeled by the CSR averaged over the hydrologically active period of the simulation (days 232–295), varied along the mainstem, with patterns reflecting spatial variability in flows during the modeled period and the effects of tributary dams on sediment supply (Figure 3). Spatial patterns of sediment balance simulated by SeRFE show similarities to long-term observations (1930s and 1940s to 2005) of channel incision and aggradation (Downs et al., 2013). Measured sediment yields suggest that the Santa Clara River basin upstream of Sespe Creek produces abundant sediment (Stillwater Sciences, 2011). Downstream of the confluences of Castaic and Piru creeks, which are dammed tributaries with reduced flood peaks, transport capacity is reduced sufficiently to cause sediment surplus (i.e., low CSR). Long-term measurements show channel aggradation in this area (Downs et al., 2013). Despite the general sediment surplus in this zone of the Santa Clara River, flow magnitudes were high enough during the 2017 flood to cause spatial heterogeneity in sediment balance. Flows were not competent to transport all sediment through this reach, resulting in zones of surplus and some deposition in reaches upstream of Sespe Creek. Between Sespe and Santa Paula creeks, the inputs of sediment and water from Sespe Creek cause the

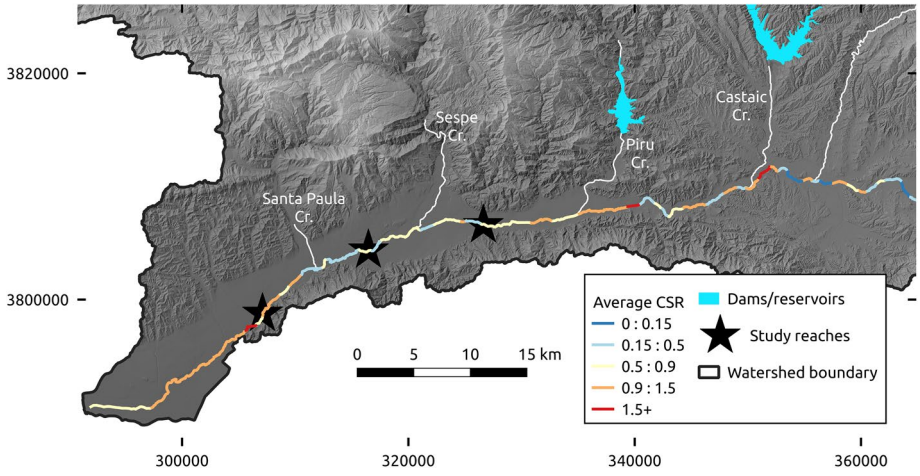

Figure 3. Capacity Supply Ratio (CSR) along the mainstem Santa Clara River, averaged for the hydrologically active period of the 2017 hydrograph. The upper reaches show the greatest sediment surplus (low CSR), the middle reaches (between Sespe and Santa Paula creeks) are approximately in equilibrium, and the downstream-most reaches are in slight sediment deficit (high CSR).

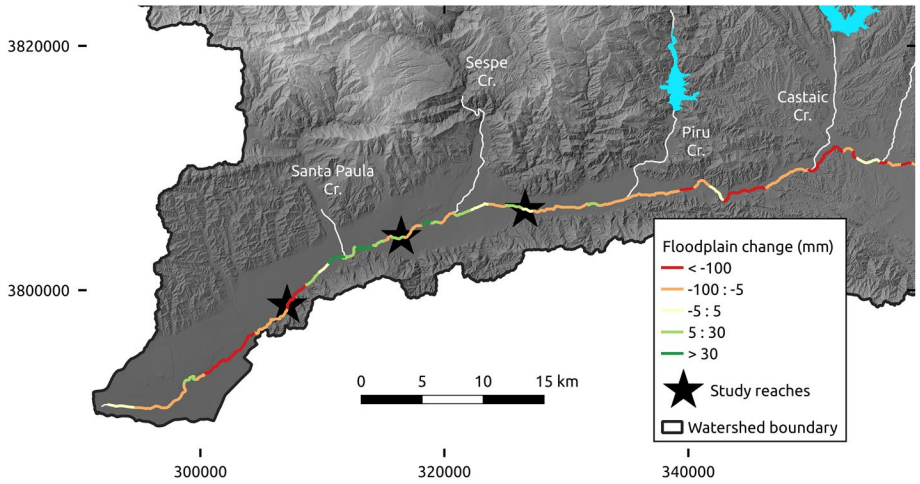

Figure 4. Sediment Routing and Floodplain Exchange (SeRFE) output for change in floodplain sediment storage, represented as a change in floodplain height. Floodplain erosion (negative values) dominated the response to the 2017 flows, with an area of deposition (positive values) in the middle reaches where floodplains are relatively wide.

sediment balance to shift closer to equilibrium; this zone has not experienced significant long-term channel incision or aggradation. Below Santa Paula Creek, the Santa Clara River is in sediment deficit because the cumulative flow and associated transport capacity exceed the sediment supply, which is reduced by sediment trapping in the upstream reservoirs. Consequently, this area has undergone incision (Downs et al., 2013).

Factors in addition to CSR cause spatial heterogeneity in channel and floodplain response to flood flows. Consequently, modeled floodplain storage changes in response to the 2017 flood differed somewhat from sediment balance and channel incision/aggradation observations (see Discussion). Although SeRFE tracks both channel and floodplain sediment storage, we focus here on floodplain storage because of its relevance to arundo production. The 5-year recurrence interval flood (based on the 2017 hydrograph) caused modeled erosion to outpace deposition for most of the basin, resulting in predominantly erosional signals in floodplain change (Figure 4). Along the mainstem Santa Clara River, the most significant floodplain erosion simulated was concentrated along the reach upstream of Piru Creek where the floodplain is relatively narrow. From the Piru Creek confluence downstream, floodplain erosion was lesser in magnitude. The only zone of significant deposition during the 2017 flood was in a sediment-surplus reach near the confluence of Santa Paula Creek, where the floodplain is relatively wide compared to reaches upstream and downstream.

3.2. Arundo Mapping and Recruitment

Arundo stands mapped in Google Earth using summer 2018 imagery aligned well with stands mapped using image classification. The total stand area differed, however, because of the different scales of our two mapping methods (1:3,000 for Google Earth classification and 1:1,000 for image classification): stand area delineated using image classification was greater than the area mapped using Google Earth (averaging 16% greater). The logistic model successfully predicted the presence of arundo stands. A model using only reach hydrology as the input resulted in 91% accuracy, while including canal intersections increased accuracy slightly to 94%. The increase was primarily a result of capturing intermittent reaches influenced by canals. The arundo recruitment potential analysis also correlated well with the mapped stand areas. Median stand area values were significantly different for each of the recruitment potential classes ($p < 0.001$; Figure 5). Median reach stand area was 0 m^2 per m of river in the low probability class, 1.7 m^2 in the moderate class and 57 m^2 in the high class.

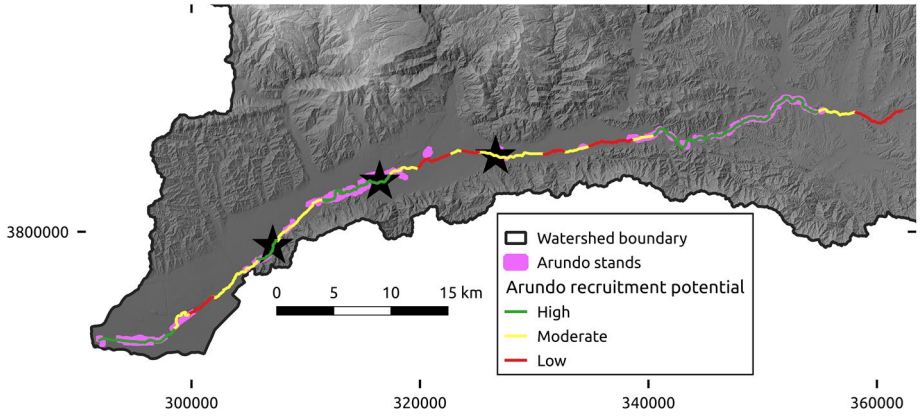

Figure 5. Output of the arundo recruitment potential analysis and the arundo stands mapped from summer 2018 imagery.

3.3. Arundo Sources and Sinks

The analysis combining the predictions of arundo recruitment potential and the modeled floodplain change highlighted distinct source and sink zones for arundo. Just upstream of the Castaic Creek confluence, there was high confidence in simulated floodplain erosion (i.e., the total range of predicted floodplain change in the output was negative), and arundo recruitment potential is high, resulting in a source zone from which arundo is eroded and transported. Downstream of this zone there are additional potential sources where floodplain erosion is modeled but confidence is not as high, or recruitment potential is not as high. In the area where deposition dominated simulated floodplain change (with high confidence), the combination of deposition and high recruitment potential causes a sink zone where transported rhizomes likely deposit and recruit. Preflood and postflood imagery from the dominant source and sink zones highlight the significant channel change and erosion occurring in the source zone, and the lack of such change in the sink zone (Figure 6).

3.4. Comparison With Validation Reaches

Comparing these modeled outputs and analysis results with the three reaches we used for model validation shows correlation between reach-scale observations and model outputs. SeRFE outputs for the upper reach simulate a small amount of deposition (Figure 7). This is consistent with imagery and DEM analysis, which show deposition in a secondary channel, along with a small degree of bank erosion and channel widening in some locations along the main channel (Figure 8). This area is within the reach affected by sediment surplus induced by flow regulation of Santa Felicia and Castaic dams, and has the lowest modeled average and maximum CSR of the study reaches (Figure 7). The reach is in an area of moderate arundo recruitment potential, and stands are present. Overall, the area of stands declined slightly between the 2007 and 2018 inventories from 22,400 to 15,900 m^2 (Figure 9). Individual plants, however, were present in the 2018 imagery along the margins of the newly deposited sediment in the secondary channel. This reach is just downstream of a reach classified as a weak/moderate arundo source, and the reduction in cover could be due to erosion and transport of Arundo from this reach.

Model outputs show the middle validation reach being in slight sediment surplus during 2017 flows, and modeled floodplain change was predominantly deposition (Figure 8). The time series of sediment storage shows that during the initial flood pulse (215 m^3/s), floodplain deposition occurred. During the second, larger flood pulse (1,200 m^3/s), additional deposition occurred, followed by erosion as flows become competent to erode the banks (Figure 7). Imagery and DEM analysis show widening of the main, low-flow channel, indicative of the erosion that occurred during the second flood peak (Figure 8). Results of hydraulic modeling using FaSTMECH show the evolution of floodplain inundation as flows approach the estimated 2017 peak flow for the reach. At 215 m^3/s, inundation of side channels and topographic low points within the floodplain occurred, and at 1,000 m^3/s, the entire floodplain was inundated (Figure 10). Mapped stands

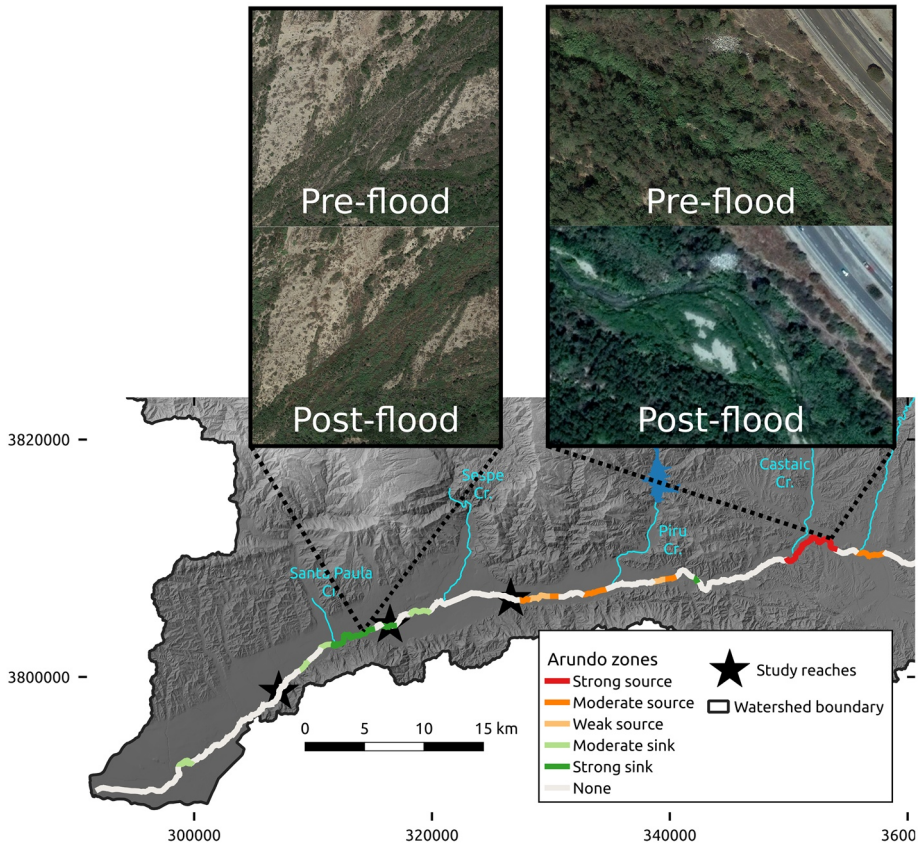

Figure 6. Results of the arundo source/sink analysis. Various weak to moderate sources of arundo are predicted throughout the middle and upper reaches of the mainstem Santa Clara River. The strongest source is in the upper reaches upstream of Castaic Creek (photos on right), and the strongest sink is just upstream of the Santa Paula Creek confluence in the middle reaches (photos on left).

for summer 2018 in this reach correspond well with portions of the floodplain inundated in the hydraulic modeling (Figures 9 and 10). This reach was classified as having high arundo recruitment potential, and between the 2007 and 2018 inventories, area of arundo stand cover increased from 7,200 to 86,600 m^2 (Figure 9).

In the lower reach, SeRFE outputs show that the average and maximum CSR values are the greatest of the three reaches. The sediment balance of the reach is in deficit, as a result of having relatively greater overall upstream flow inputs (from Sespe and Santa Paula creeks) than sediment inputs (due to reservoir sediment trapping further upstream on Castaic and Piru creeks). Floodplain change was dominated by erosion, and imagery suggests erosion of the large bar along this reach occurred (Figure 8). Change in arundo coverage was minimal. A large, persistent stand present since after the large 2005 floods remained virtually the same between 2007 and 2018 (Figure 9).

4. Discussion

Process-based restoration of rivers and riparian ecosystems targets root causes of degradation, accounts for sediment balances and connectivity, and couples watershed-scale planning, actions, and perspectives with reach-scale efforts (e.g., Beechie et al., 2010). A watershed-scale approach to arundo removal and treatment, for example, would be grounded in recognition of arundo's clonal reproduction, as well as sediment connectivity, and would thus ideally be implemented from the top of a watershed down (Bell, 1998; Quinn & Holt, 2009). Fully realizing this approach in complex river basins with varied ownership like the Santa Clara may not be feasible, but strategic, targeted efforts can still achieve restoration objectives. Indeed, limited funding and resources for restoration demand such targeted efforts, and application of models such as SeR-

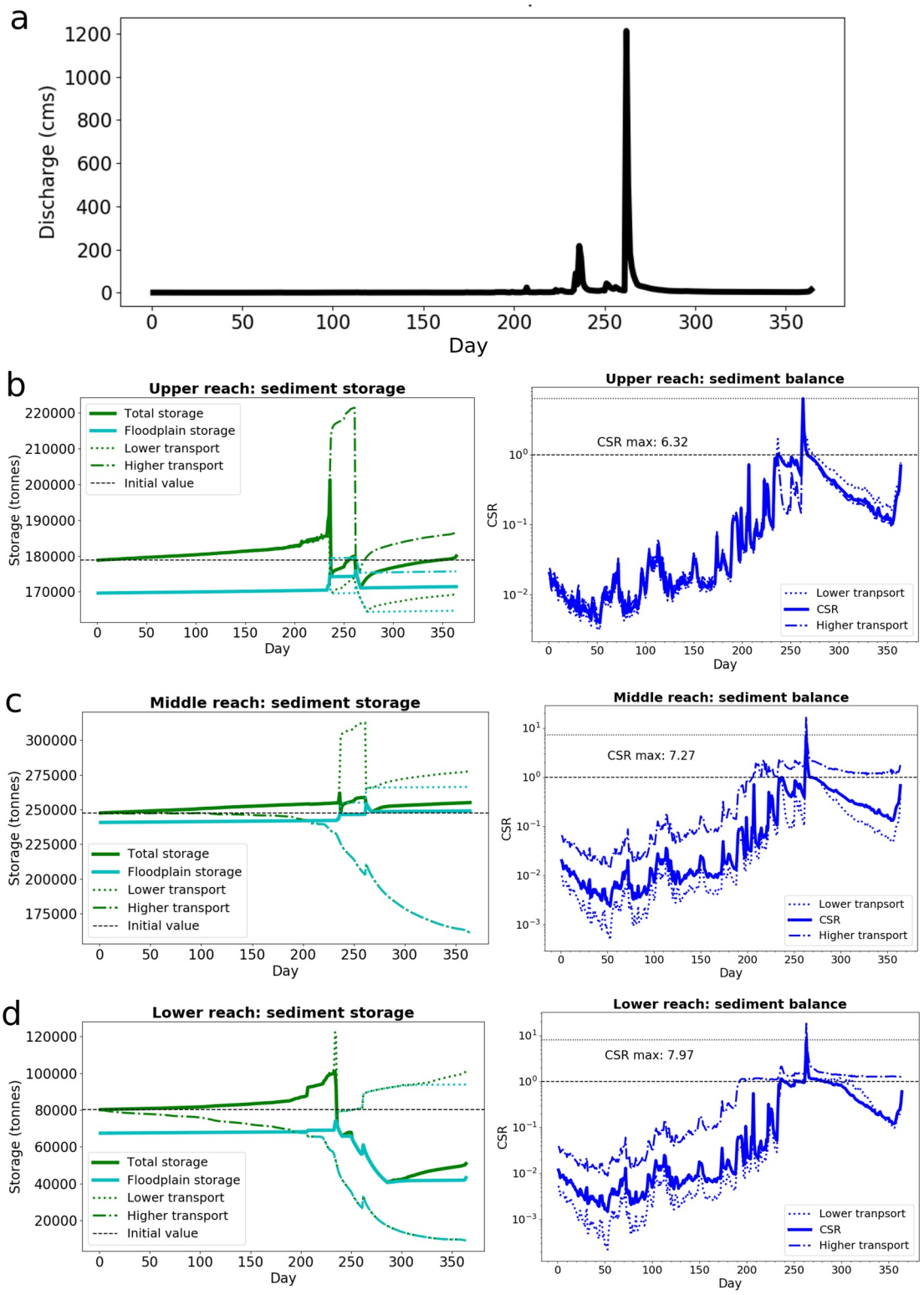

Figure 7. Santa Clara River Sediment Routing and Floodplain Exchange (SeRFE) simulation hydrograph (summer 2016-summer 2017) for the lower study reach (a), and SeRFE model outputs for simulated sediment storage and the Capacity Supply ratio (CSR) for the upper (b), middle (c), and lower (d) study reaches. The lower transport and higher transport scenarios in the charts represent the range of uncertainty based on the prediction range of median grain size for the reach.

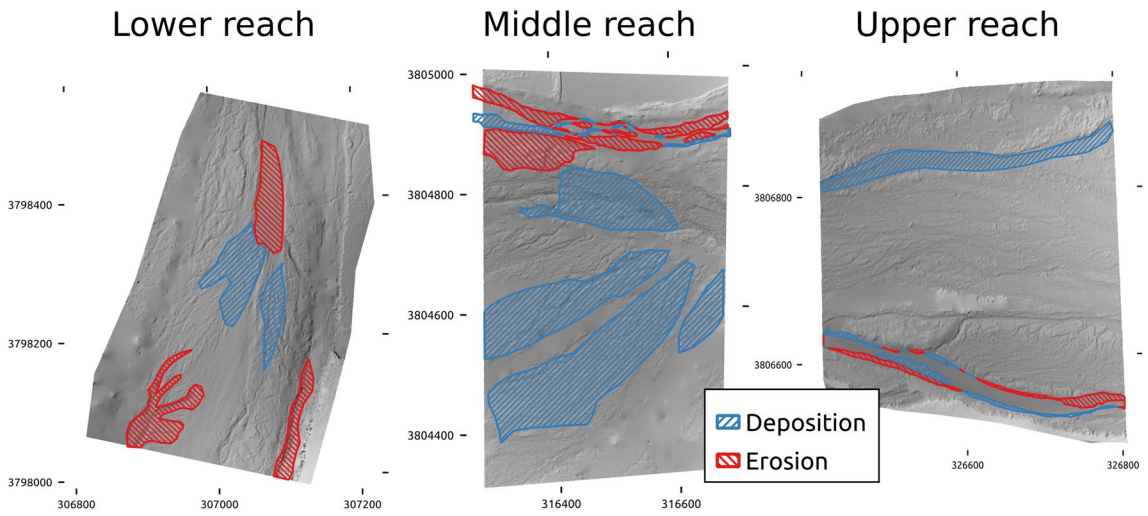

Figure 8. Geomorphic change from digital elevation model (DEM) and orthophoto comparison between 2015 and 2018 at the three validation reaches. More erosion occurred than deposition in the lower reach, while deposition dominated in the middle reach. Changes in the upper reach were smaller in magnitude, but some deposition occurred in a side channel.

FE can contribute to strategic, watershed-scale restoration planning. The SeRFE modeling presented here illustrates how arundo source areas can be identified and provides a geomorphic-process basis for focusing on particular source areas to improve the efficacy of restoration treatments. In the case of the Santa Clara River, our results suggest that reaches upstream of Piru Creek are primarily acting as sources for recruitment in depositional areas lower in the watershed. Our results can also help to prioritize among potential restoration areas downstream of arundo propagule sources that are relatively more or less susceptible to recruitment and regeneration. Watershed-scale, spatially explicit perspectives about relationships between vegetation source areas and restoration target areas, and of sediment balances and storage, such as provided by the findings presented here, are broadly applicable to riparian restoration in the face of invasive, clonally reproducing species.

Our coupled, watershed-scale sediment and vegetation modeling also advances fluvial-process understanding with respect to expected ecogeomorphic responses of riparian and floodplain systems to differing vegetation and sediment balance conditions. Whereas changes to sediment balance have been linked to channel

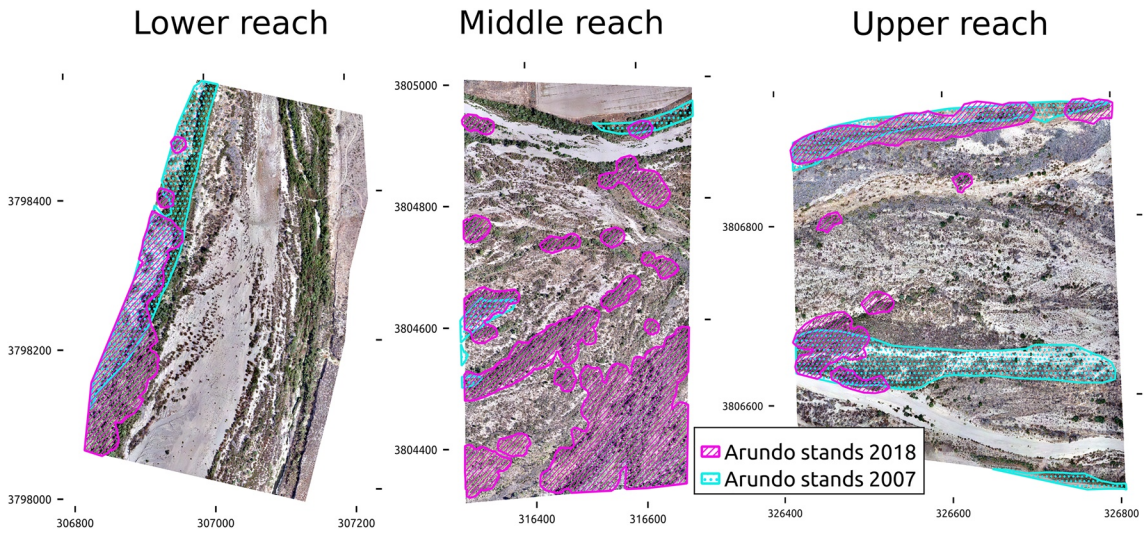

Figure 9. Comparison of arundo stand cover at the three study reaches between 2007 and 2018. Imagery from 2018. There was no significant change in arundo stand area in the lower reach. The middle reach experienced a large increase in stand area, and the upper reach a small decrease.

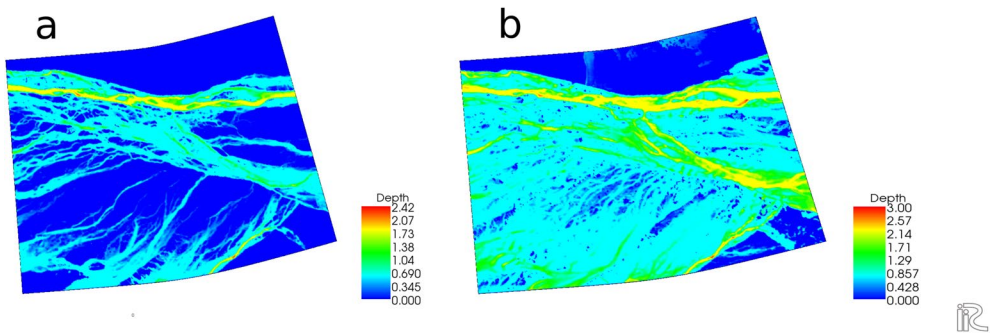

Figure 10. FaSTMECH hydrologic modeling outputs for the middle study reach at the two peak discharge values simulated in the 2017 hydrographs. At 215 m^3/s (a), some floodplain inundation has occurred, and at 1,000 m^3/s (b), all but the highest portions of the floodplain are inundated.

incision and aggradation (e.g., Schmidt & Wilcock, 2008), their effect on floodplains is less understood. In this study, general patterns of average CSR correlated with patterns of long-term channel aggradation and incision. For the annual or event-level temporal scale modeled here, however, floodplain change was more strongly correlated with maximum CSR (i.e., the largest CSR value for the segment during the simulation; $r^2 = 0.37$) than with average CSR ($r^2 = 0.15$). This correlation indicates that sediment balance during short, peak flows plays a role in floodplain response: whereas sediment transport capacity is maximized at peak-flow conditions, floodplain erosion under these conditions produces additional supply, minimizing imbalances between transport capacity and supply and stabilizing the CSR. Network topology also influences floodplain change, which at a given segment correlates with both the maximum CSR of the next segment upstream ($r^2 = 0.25$) and with change in floodplain sediment storage upstream ($r^2 = 0.25$). In summary, model outputs suggest that floodplain erosion, deposition, and therefore changes in sediment storage, are controlled by the factors that affect the maximum CSR, including upstream sediment supply and stream power (peak flow magnitude and channel geometry).

The analysis presented here of how sediment balance (as expressed by CSR) relates to channel and floodplain geomorphic change at different time scales complements laboratory studies investigating how sediment balance mediates ecogeomorphic feedbacks. For example, Lightbody et al. (2019) found that topographic change on bars was insensitive to vegetation density and morphology under sediment-deficit conditions (high CSR), in contrast to the strong influence of vegetation on deposition observed under equilibrium supply. Diehl, Merritt, et al. (2017) and Diehl, Wilcox, et al. (2017) also documented differences in how vegetation size and morphology influenced bar-surface topography for sediment deficit versus equilibrium conditions. Those and other laboratory studies are especially adept at explicitly representing vegetation-related feedbacks on morphodynamics at plant to bar scales. The modeling presented here expands insights into the interactions between flow, sediment supply, vegetation, and geomorphic change to broader scales of time (i.e., across annual hydrographs) and space (i.e., across channel networks and between channels and floodplains). Our modeling thus illustrates how longitudinal and lateral connectivity of both sediment and arundo mediate morphodynamic change.

In the Santa Clara River, floodplain erosion was modeled along the river upstream of Piru Creek, where channel slopes are the highest and widths the narrowest, causing the highest maximum CSR values (~10–-25). This zone of floodplain erosion coincides with conditions favorable for arundo recruitment, resulting in our identified source zone. Between Piru Creek and Sespe Creek, maximum CSR values decline as slopes decrease and tributary flow regulation reduces peak flows. Floodplain change here varied, with alternating erosion and aggradation based on local conditions. Below Sespe Creek, sediment contributions from unregulated tributaries and the lowest channel slopes and widest floodplains along the river result in the lowest CSR values (~6–7; e.g., the middle validation reach). This reach was dominated by floodplain deposition and overlaps with areas of high arundo recruitment potential, resulting in the sink area for rhizomes identified in our analysis. This area has undergone a rapid expansion in arundo stand cover since the last flood large enough to remove all vegetation (2005; see middle reach in Figure 9). Patches of arundo in this area, and several other areas downstream have been treated with herbicide and mowed, in order to remove it, but

success has been variable, and in some cases, stands have regenerated, or new propagules have recruited in the same areas. Our analysis suggests this may be due to the sediment dynamics, as well as an upstream source that has not been treated, and reinforces existing recommendations of selecting treatment reaches based on their geomorphic characteristics and hydrology. We also note that the region experienced a severe drought in the years preceding this study (2012 to early 2017), and arundo leaf loss during drought may have reduced its visibility on aerial imagery. This could account for some of the reduction in arundo area in the upper reach. Similarly, a return to moister conditions coinciding with this study could be a factor in the expansion in stand area in the middle reach.

In coupled modeling frameworks such as the one presented here, limitations of each model component must be considered. Our approach is primarily founded on a sediment model (SeRFE), to focus on the geomorphic drivers of arundo dynamics, which is then coupled with an arundo recruitment potential model based on groundwater and nutrients. We do not address additional factors that could influence recruitment, such as soil characteristics, depth of deposition, timing of deposition, underground rhizome propagation that expands existing stands, and root formation from fallen culms (Boland, 2006). At the reach scales we use for modeling, however, our logistic model predicted reaches where arundo stands occurred quite well (94% accuracy).

SeRFE accounts for uncertainty in model outputs by quantifying error in median grain size estimates from bed grain size measurements using a prediction interval, and propagating that error through the modeling process. Reaches that are closer to measurement locations and that have a narrower range of bed grain sizes therefore have much less uncertainty in their outputs than reaches that are farther from measurements and have a wide range of bed grain sizes. For example, the sediment storage and CSR outputs have much narrower prediction intervals in the upper validation reach, where confidence in median grain size is higher than in the lower reach (Figure 7). Bank erodibility can be highly spatially variable, owing in part to riparian vegetation and root density, which also produces uncertainty in network-scale modeling. We expect that our extrapolation of values of k, the erodibility factor in Equation 3, based on measured values of critical stream power at a few reaches, results in underestimates of bank erosion in areas with sparse vegetation, or where riparian vegetation is comprised primarily of species with shallow rooting depths like arundo. Conversely, bank erosion may be overestimated along reaches flanked by woody species. For example, along a 10 km reach of the upper Santa Clara River where floodplain width is relatively uniform, image analysis suggests that more bank erosion occurred in the portion where arundo stands were denser. At the watershed scale, the distribution of sparse versus dense riparian vegetation would influence the sensitivity of model results to the assumption of a constant relationship between ω_c and k, and thus the extent to which overestimates and underestimates of bank erosion are offsetting. Future model improvements could explicitly incorporate the influence of vegetation on bank erosion using geospatial datasets of riparian species and extent. For a more complete discussion on limitations and assumptions of the SeRFE model, see Gilbert and Wilcox (2020).

Generally, the level of detail required to parameterize fully coupled ecogeomorphic models constrains their application to reach-scale modeling domains (e.g., Diehl et al., 2018). The approach presented here sacrifices the detail of such reach-scale approaches in favor of spatially explicit modeling of entire drainage basins that, as a result, represents connectivity with upstream portions of the basin and its resulting downstream impacts. In this application, floodplain geomorphic change depends in part on the flux of sediment from upstream, which is a function of both the spatially variable upstream hillslope supply as well as bank erosion. Because floodplain change is a dominant control on arundo spread, modeling these topological effects on sediment dynamics for each reach is important for achieving accurate results at the basin scale. Effective restoration treatments are generally applied at reach scales, therefore, this method of identifying reaches based on basin-scale modeling is particularly valuable.

Explicitly incorporating advances in understanding of physical processes occurring at the plant-flow interface at fine scales, and scaling up representations of these processes in order to incorporate them into basin-scale modeling approaches, represent key avenues for future study. For example, in a review of research investigating interactions between the riparian Salicaceae family and hydrogeomorphic processes, Politti et al. (2018) highlight flow resistance of flexible plant parts and leaves, the increase in cohesive properties vegetation adds to alluvial soils, and plant flooding tolerance as areas where increased understanding would enable improved modeling of these processes. Similarly, Camporeale et al. (2013) emphasize the need for

ecogeomorphic modeling to consider vegetation from a process-based biological perspective rather than as a static element in its influence of hydrodynamics.

While this study focused on applying a coupled ecogeomorphic model to the problem of arundo invasion in the Santa Clara River, the example approach could be applied elsewhere where invasive plants are a management concern, and serves as a template for combining other sediment and ecological models to address ecogeomorphic restoration and management concerns. Our results suggest that in cases where the primary relevant geomorphic and ecological processes can be simulated, coupling the two can provide insights that would not be achieved using either type of model alone.

5. Conclusion

The combined sediment and vegetation modeling presented here provides a framework to inform restoration and understand ecogeomorphic interactions within watersheds. In our application of this approach to the Santa Clara River, where bank erosion and arundo dynamics are coupled, we combined spatially explicit bank erosion modeling with arundo stand locations to assess how flood flows are potentially redistributing the vegetation within the catchment. Specifically, areas of the watershed that we modeled as having high sediment transport capacity relative to supply, favorable conditions for arundo recruitment, and high floodplain erosion represent arundo source zones, whereas areas modeled to have higher sediment supply, floodplain deposition, and arundo recruitment potential represent arundo sink areas.

Channel-network scale results regarding both invasive-species sources and sinks and sediment balances link longitudinal and lateral connectivity of both sediment and arundo to morphodynamic change. We show that floodplain change is correlated both to the sediment balance in upstream reaches, illustrating sediment-connectivity effects on geomorphic adjustment, and to the sediment balance at peak flows, when high transport capacity and floodplain erosion may have offsetting effects that stabilize sediment balance and thus maintain a tendency toward morphodynamic equilibrium. Models linking sediment and vegetation, and more generally that couple physical and ecological processes, are essential for advancing understanding of river-floodplain processes and for informing management and restoration of those systems in the face of species invasions, climate change, and other stresses.

Data Availability Statement

A combination of publicly available datasets and datasets the authors generated were used for these analyses. They used the National Elevation Data set (NED) available through the USGS for 10m DEMs, and the National Hydrography Datasets (NHD) for stream networks and canals. They used the National Land Cover Data set (NLCD) for land cover classification. 2007 vegetation datasets and 1m DEMs for the mainstem Santa Clara River were provided by Stillwater Sciences. The remaining data the authors used for the Arundo recruitment model and to calibrate and run the SeRFE model for the application presented here are available at the DOI http://doi.org/10.5281/zenodo.4408509, including grain size measurements adapted from both USGS and Stillwater Sciences measurements.

Acknowledgments
This manuscript is based upon work supported by UM BRIDGES through funding from the National Science Foundation under Grant No. DGE-1633831 and by NSF EAR-1644619. The authors thank Eric Hallstein, Judah Grossman, Laura Riege, and Jeanette Howard of The Nature Conservancy California for their contributions to this work. Additionally, they thank Ben Colman, Marco Maneta, Amy East, and three anonymous reviewers for helpful reviews of this manuscript.

References

Andrews, E. D., Antweiler, R. C., Neiman, P. J., & Ralph, F. M. (2004). Influence of ENSO on flood frequency along the California coast. *Journal of Climate*, *17*, 337–348. https://doi.org/10.1175/1520-0442(2004)017<0337:ioeoff>2.0.co;2

Beechie, T. J., Sear, D. A., Olden, J. D., Pess, G. R., Buffington, J. M., Moir, H., et al. (2010). Process-based principles for restoring river ecosystems. *BioScience*, *60*, 209–222. https://doi.org/10.1525/bio.2010.60.3.7

Bell, G. P. (1998). *Ecology and management of Arundo donax, and approaches to riparian habitat restoration in southern California* (pp. 103–113). Backhuys Publishers.

Bertoldi, W., Siviglia, A., Tettamanti, S., Toffolon, M., Vetsch, D., & Francalanci, S. (2014). Modeling vegetation controls on fluvial morphological trajectories. *Geophysical Research Letters*, *41*, 7167–7175. https://doi.org/10.1002/2014gl061666

Boland, J. M. (2006). The importance of layering in the rapid spread of Arundo donax (giant reed). *Madroño*, *53*, 303–312. https://doi.org/10.3120/0024-9637(2006)53[303:tiolit]2.0.co;2

Boose, A. B., & Holt, J. S. (1999). Environmental effects on asexual reproduction in Arundo donax. *Weed Research*, *39*, 117–127. https://doi.org/10.1046/j.1365-3180.1999.00129.x

Booth, D. B., Leverich, G., Downs, P. W., Dusterhoff, S., & Araya, S. (2014). A method for spatially explicit representation of sub-watershed sediment yield, Southern California, USA. *Environmental Management*, *53*, 968–984. https://doi.org/10.1007/s00267-014-0251-9

Burton, C. A., Montrella, J., Landon, M. K., & Belitz, K. (2011). *Status and understanding of groundwater quality in the Santa Clara River valley, 2007-California GAMA priority basin project* (p. 67). U. S. Geological Survey. https://doi.org/10.3133/sir20115052

Bywater-Reyes, S., Wilcox, A. C., Stella, J. C., & Lightbody, A. F. (2015). Flow and scour constraints on uprooting of pioneer woody seedlings. *Water Resources Research*, *51*, 9190–9206. https://doi.org/10.1002/2014WR016641

Cadol, D., Rathburn, S. L., & Cooper, D. J. (2011). Aerial photographic analysis of channel narrowing and vegetation expansion in Canyon de Chelly National Monument, Arizona, USA, 1935 - 2004. *River Research and Applications*, *27*, 841–856. https://doi.org/10.1002/rra.1399

Camporeale, C., Perucca, E., Ridolfi, L., & Gurnell, A. M. (2013). Modeling the interactions between river morphodynamics and riparian vegetation. *Reviews of Geophysics*, *51*, 379–414. https://doi.org/10.1002/rog.20014

Caponi, F., Vetsch, D. F., & Siviglia, A. (2020). A model study of the combined effect of above and below ground plant traits on the ecomorphodynamics of gravel bars. *Scientific Reports*, *10*, 1–14. https://doi.org/10.1038/s41598-020-74106-9

Coffman, G. C. (2007). *Factors influencing invasion of giant reed (Arundo donax) in riparian ecosystems of Mediterranean-type climate regions*. University of California. https://doi.org/10.13140/RG.2.2.30890.16324

Coffman, G. C., Ambrose, R. F., & Rundel, P. W. (2010). Wildfire promotes dominance of invasive giant reed (Arundo donax) in riparian ecosystems. *Biological Invasions*, *12*, 2723–2734. https://doi.org/10.1007/s10530-009-9677-z

Corenblit, D., Tabacchi, E., Steiger, J., & Gurnell, A. M. (2007). Reciprocal interactions and adjustments between fluvial landforms and vegetation dynamics in river corridors: A review of complementary approaches. *Earth-Science Reviews*, *84*, 56–86. https://doi.org/10.1016/j.earscirev.2007.05.004

Couper, P. (2003). Effects of silt–clay content on the susceptibility of river banks to subaerial erosion. *Geomorphology*, *56*(1–2), 95–108. https://doi.org/10.1016/s0169-555x(03)00048-5

Crosato, A., & Saleh, M. S. (2011). Numerical study on the effects of floodplain vegetation on river planform style. *Earth Surface Processes and Landforms*, *36*, 711–720. https://doi.org/10.1002/esp.2088

Cushman, J. H., & Gaffney, K. A. (2010). Community-level consequences of invasion: Impacts of exotic clonal plants on riparian vegetation. *Biological Invasions*, *12*, 2765–2776. https://doi.org/10.1007/s10530-009-9682-2

Darby, S. E., Rinaldi, M., & Dapporto, S. (2007). Coupled simulations of fluvial erosion and mass wasting for cohesive river banks. *Journal of Geophysical Research*, *112*. https://doi.org/10.1029/2006jf000722

Decruyenaere, J. G., & Holt, J. S. (2005). Ramet demography of a clonal invader, Arundo donax (Poaceae), in southern California. *Plant and Soil*, *277*, 41–52. https://doi.org/10.1007/s11104-005-0264-5

Diehl, R. M., Merritt, D. M., Wilcox, A. C., & Scott, M. L. (2017). Applying functional traits to ecogeomorphic processes in riparian ecosystems. *BioScience*, *67*, 729–743. https://doi.org/10.1093/biosci/bix080

Diehl, R. M., Wilcox, A. C., Merritt, D. M., Perkins, D. W., & Scott, J. A. (2018). Development of an eco-geomorphic modeling framework to evaluate riparian ecosystem response to flow-regime changes. *Ecological Engineering*, *123*, 112–126. https://doi.org/10.1016/j.ecoleng.2018.08.024

Diehl, R. M., Wilcox, A. C., Stella, J. C., Kui, L., Sklar, L. S., & Lightbody, A. (2017). Fluvial sediment supply and pioneer woody seedlings as a control on bar-surface topography. *Earth Surface Processes and Landforms*, *42*, 724–734. https://doi.org/10.1002/esp.4017

Downs, P. W., Dusterhoff, S. R., & Sears, W. A. (2013). Reach-scale channel sensitivity to multiple human activities and natural events: Lower Santa Clara River, California, USA. *Geomorphology*, *189*, 121–134. https://doi.org/10.1016/j.geomorph.2013.01.023

Dudley, T. L. (2000). Arundo donax. In C. C. Bossard, J. M. Randall, & M. C. Hoshovsky (Eds.), *Invasive plants of California's wildlands* (pp. 53–58). University of California Press.

Fernandes, M. R., Aguiar, F. C., Silva, J. M., Ferreira, M. T., & Pereira, J. M. (2013). Spectral discrimination of giant reed (Arundo donax L.): A seasonal study in riparian areas. *ISPRS Journal of Photogrammetry and Remote Sensing*, *80*, 80–90. https://doi.org/10.1016/j.isprsjprs.2013.03.007

Florsheim, J. L., Keller, E. A., & Best, D. W. (1991). Fluvial sediment transport in response to moderate storm flows following chaparral wildfire, Ventura county, southern California. *Geological Society of America Bulletin*, *103*, 504–511. https://doi.org/10.1130/0016-7606(1991)103<0504:fstirt>2.3.co;2

Fraaije, R. G., ter Braak, C. J., Verduyn, B., Verhoeven, J. T., & Soons, M. B. (2015). Dispersal versus environmental filtering in a dynamic system: Drivers of vegetation patterns and diversity along stream riparian gradients. *Journal of Ecology*, *103*, 1634–1646. https://doi.org/10.1111/1365-2745.12460

Friedman, J. M., Auble, G. T., Shafroth, P. B., Scott, M. L., Merigliano, M. F., Freehling, M. D., & Griffin, E. R. (2005). Dominance of non-native riparian trees in western USA. *Biological Invasions*, *7*, 747–751. https://doi.org/10.1007/s10530-004-5849-z

Gilbert, J. T., & Wilcox, A. C. (2020). Sediment routing and floodplain exchange (SeRFE): A spatially explicit model of sediment balance and connectivity through river networks. *Journal of Advances in Modeling Earth Systems*, *12*, e2020MS002048. https://doi.org/10.1029/2020ms002048

Gran, K., & Paola, C. (2001). Riparian vegetation controls on braided stream dynamics. *Water Resources Research*, *37*, 3275–3283. https://doi.org/10.1029/2000wr000203

Gurnell, A. M., Bertoldi, W., & Corenblit, D. (2012). Changing river channels: The roles of hydrological processes, plants and pioneer fluvial landforms in humid temperate, mixed load, gravel bed rivers. *Earth-Science Reviews*, *111*, 129–141. https://doi.org/10.1016/j.earscirev.2011.11.005

Hardion, L., Verlaque, R., Saltonstall, K., Leriche, A., & Vila, B. (2014). Origin of the invasive Arundo donax (Poaceae): A trans-asian expedition in herbaria. *Annals of Botany*, *114*, 455–462. https://doi.org/10.1093/aob/mcu143

Hooke, J. M., Brookes, C. J., Duane, W., & Mant, J. M. (2005). A simulation model of morphological, vegetation and sediment changes in ephemeral streams. *Earth Surface Processes and Landforms*, *30*, 845–866. https://doi.org/10.1002/esp.1195

Hough-Snee, N., Laub, B. G., Merritt, D. M., Long, A. L., Nackley, L. L., Roper, B. B., & Wheaton, J. M. (2015). Multi-scale environmental filters and niche partitioning govern the distributions of riparian vegetation guilds. *Ecosphere*, *6*, 1–22. https://doi.org/10.1890/es15-00064.1

Janes, V., Nicholas, A. P., Collins, A. L., & Quine, T. A. (2017). Analysis of fundamental physical factors influencing channel bank erosion: Results for contrasting catchments in England and wales. *Environmental Earth Sciences*, *76*, 307. https://doi.org/10.1007/s12665-017-6593-x

Keeley, J. E., & Fotheringham, C. J. (2001). Historic fire regime in southern california shrublands. *Conservation Biology*, *15*, 1536–1548. https://doi.org/10.1046/j.1523-1739.2001.00097.x

Kelley, E. (2004). *Information synthesis and priorities regarding steelhead trout (Oncorhynchus mykiss) on the Santa Clara River*. Santa Barbara: University of California. prepared for The Nature Conservancy.

Khanal, A., Klavon, K. R., Fox, G. A., & Daly, E. R. (2016). Comparison of linear and nonlinear models for cohesive sediment detachment: Rill erosion, hole erosion test, and streambank erosion studies. *Journal of Hydraulic Engineering*, *142*, 04016026. https://doi.org/10.1061/(asce)hy.1943-7900.0001147

Klavon, K., Fox, G., Guertault, L., Langendoen, E., Enlow, H., Miller, R., & Khanal, A. (2017). Evaluating a process-based model for use in streambank stabilization: Insights on the bank stability and toe erosion model (BSTEM). *Earth Surface Processes and Landforms*, *42*, 191–213. https://doi.org/10.1002/esp.4073

Kui, L., & Stella, J. C. (2016). Fluvial sediment burial increases mortality of young riparian trees but induces compensatory growth response in survivors. *Forest Ecology and Management*, *366*, 32–40. https://doi.org/10.1016/j.foreco.2016.02.001

Kus, B. E. (1998). Use of restored riparian habitat by the endangered least bell's vireo (vireo bellii pusillus). *Restoration Ecology*, *6*, 75–82. https://doi.org/10.1046/j.1526-100x.1998.06110.x

Lambert, A. M., Dudley, T. L., & Robbins, J. (2014). Nutrient enrichment and soil conditions drive productivity in the large-statured invasive grass Arundo donax. *Aquatic Botany*, *112*, 16–22. https://doi.org/10.1016/j.aquabot.2013.07.004

Lambert, A. M., Dudley, T. L., & Saltonstall, K. (2010). Ecology and impacts of the large-statured invasive grasses Arundo donax and Phragmites australis in North America. *Invasive Plant Science and Management*, *3*, 489–494. https://doi.org/10.1614/ipsm-d-10-00031.1

Lammers, R. W., & Bledsoe, B. P. (2018). Parsimonious sediment transport equations based on Bagnold's stream power approach. *Earth Surface Processes and Landforms*, *43*, 242–258. https://doi.org/10.1002/esp.4237

Larsen, E. W., Premier, A. K., & Greco, S. E. (2006). Cumulative effective stream power and bank erosion on the Sacramento River, California, USA. *JAWRA Journal of the American Water Resources Association*, *42*, 1077–1097. https://doi.org/10.1111/j.1752-1688.2006.tb04515.x

Lightbody, A. F., Kui, L., Stella, J. C., Skorko, K. W., Bywater-Reyes, S., & Wilcox, A. C. (2019). Riparian vegetation and sediment supply regulate the morphodynamic response of an experimental stream to floods. *Frontiers in Environmental Science*, *7*, 40. https://doi.org/10.3389/fenvs.2019.00040

Maceda-Veiga, A., Basas, H., Lanzaco, G., Sala, M., de Sostoa, A., & Serra, A. (2016). Impacts of the invader giant reed (Arundo donax) on riparian habitats and ground arthropod communities. *Biological Invasions*, *18*, 731–749. https://doi.org/10.1007/s10530-015-1044-7

Manners, R. B., Schmidt, J., & Wheaton, J. M. (2013). Multiscalar model for the determination of spatially explicit riparian vegetation roughness. *Journal of Geophysical Research*, *118*, 65–83. https://doi.org/10.1029/2011jf002188

Manners, R. B., Wilcox, A. C., Kui, L., Lightbody, A. F., Stella, J. C., & Sklar, L. S. (2015). When do plants modify fluvial processes? plant-hydraulic interactions under variable flow and sediment supply rates. *Journal of Geophysical Research: Earth Surface*, *120*, 325–345. https://doi.org/10.1002/2014jf003265

Martinez, A. E., & McDowell, P. F. (2016). Invasive reed canarygrass (Phalaris arundinacea) and native vegetation channel roughness. *Invasive Plant Science and Management*, *9*, 12–21. https://doi.org/10.1614/ipsm-d-15-00046.1

McShane, R. R., Auerbach, D. A., Friedman, J. M., Auble, G. T., Shafroth, P. B., Merigliano, M. F., et al. (2015). Distribution of invasive and native riparian woody plants across the western USA in relation to climate, river flow, floodplain geometry and patterns of introduction. *Ecography*, *38*, 1254–1265. https://doi.org/10.1111/ecog.01285

Merritt, D. M., Scott, M. L., LeRoy Poff, N., Auble, G. T., & Lytle, D. A. (2010). Theory, methods and tools for determining environmental flows for riparian vegetation: Riparian vegetation-flow response guilds. *Freshwater Biology*, *55*, 206–225. https://doi.org/10.1111/j.1365-2427.2009.02206.x

Micheli, E. R., Kirchner, J. W., & Larsen, E. W. (2004). Quantifying the effect of riparian forest versus agricultural vegetation on river meander migration rates, central Sacramento River, California, USA. *River Research and Applications*, *20*, 537–548. https://doi.org/10.1002/rra.756

Millar, R. G. (2000). Influence of bank vegetation on alluvial channel patterns. *Water Resources Research*, *36*, 1109–1118. https://doi.org/10.1029/1999wr900346

Millar, R. G. (2005). Theoretical regime equations for mobile gravel-bed rivers with stable banks. *Geomorphology*, *64*, 207–220. https://doi.org/10.1016/j.geomorph.2004.07.001

Nelson, J. M., Shimizu, Y., Abe, T., Asahi, K., Gamou, M., Inoue, T., et al. (2016). The international river interface cooperative: Public domain flow and morphodynamics software for education and applications. *Advances in Water Resources*, *93*, 62–74. https://doi.org/10.1016/j.advwatres.2015.09.017

Orme, A. R. (1999). Late quaternary tectonism along the pacific coast of the Californias: A contrast in style. *Geological Society, London, Special Publications*, *146*, 179–197. https://doi.org/10.1144/gsl.sp.1999.146.01.10

Osterkamp, W. R., & Hupp, C. R. (2010). Fluvial processes and vegetation: Glimpses of the past, the present, and perhaps the future. *Geomorphology*, *116*, 274–285. https://doi.org/10.1016/j.geomorph.2009.11.018

Parker, C., Clifford, N. J., & Thorne, C. R. (2011). Understanding the influence of slope on the threshold of coarse grain motion: Revisiting critical stream power. *Geomorphology*, *126*, 51–65. https://doi.org/10.1016/j.geomorph.2010.10.027

Parker, G., Shimizu, Y., Wilkerson, G. V., Eke, E. C., Abad, J. D., Lauer, J. W., et al. (2011). A new framework for modeling the migration of meandering rivers. *Earth Surface Processes and Landforms*, *36*, 70–86. https://doi.org/10.1002/esp.2113

Parker, S. S., Remson, E. J., & Verdone, L. N. (2014). Restoring conservation nodes to enhance biodiversity and ecosystem function along the Santa Clara River. *Ecological Restoration*, *32*, 6–8. https://doi.org/10.3368/er.32.1.6

Parker, S. S., Verdone, L. N., Remson, E. J., & Cohen, B. S. (2016). Prioritizing riparian conservation: A methodology developed for the Santa Clara River, California. *Ecological Restoration*, *34*, 61–67. https://doi.org/10.3368/er.34.1.61

Partheniades, E. (1965). Erosion and deposition of cohesive soils. *Journal of the Hydraulics Division*, *91*, 105–139. https://doi.org/10.1061/jyceaj.0001165

Perucca, E., Camporeale, C., & Ridolfi, L. (2007). Significance of the riparian vegetation dynamics on meandering river morphodynamics. *Water Resources Research*, *43*. https://doi.org/10.1029/2006wr005234

Pizzuto, J. E., & Meckelnburg, T. S. (1989). Evaluation of a linear bank erosion equation. *Water Resources Research*, *25*, 1005–1013. https://doi.org/10.1029/wr025i005p01005

Politti, E., Bertoldi, W., Gurnell, A., & Henshaw, A. (2018). Feedbacks between the riparian salicaceae and hydrogeomorphic processes: A quantitative review. *Earth-Science Reviews*, *176*, 147–165. https://doi.org/10.1016/j.earscirev.2017.07.018

Pollen-Bankhead, N., & Simon, A. (2010). Hydrologic and hydraulic effects of riparian root networks on streambank stability: Is mechanical root-reinforcement the whole story? *Geomorphology*, *116*, 353–362. https://doi.org/10.1016/j.geomorph.2009.11.013

Quinn, L. D., & Holt, J. S. (2008). Ecological correlates of invasion by Arundo donax in three southern California riparian habitats. *Biological Invasions*, *10*, 591–601. https://doi.org/10.1007/s10530-007-9155-4

Quinn, L. D., & Holt, J. S. (2009). Restoration for resistance to invasion by giant reed (Arundo donax). *Invasive Plant Science and Management*, *2*, 279–291. https://doi.org/10.1614/ipsm-09-001.1

Richardson, D. M., Holmes, P. M., Esler, K. J., Galatowitsch, S. M., Stromberg, J. C., Kirkman, S. P., et al. (2007). Riparian vegetation: Degradation, alien plant invasions, and restoration prospects. *Diversity and Distributions*, *13*, 126–139. https://doi.org/10.1111/j.1366-9516.2006.00314.x

Rowntree, K. (1991). An assessment of the potential impact of alien invasive vegetation on the geomorphology of river channels in South Africa. *Southern African Journal of Aquatic Sciences*, *17*, 28–43. https://doi.org/10.1080/10183469.1991.9631311

Saltonstall, K., Lambert, A., & Meyerson, L. A. (2010). Genetics and reproduction of common (Phragmites australis) and giant reed (Arundo donax). *Invasive Plant Science and Management*, *3*, 495–505. https://doi.org/10.1614/ipsm-09-053.1

Schmidt, J. C., & Wilcock, P. R. (2008). Metrics for assessing the downstream effects of dams. *Water Resources Research*, *44*. https://doi.org/10.1029/2006wr005092

Shields, F. D., Jr, Coulton, K. G., & Nepf, H. (2017). Representation of vegetation in two-dimensional hydrodynamic models. *Journal of Hydraulic Engineering*, *143*, 02517002. https://doi.org/10.1061/(asce)hy.1943-7900.0001320

Simon, A., Curini, A., Darby, S. E., & Langendoen, E. J. (2000). Bank and near-bank processes in an incised channel. *Geomorphology*, *35*, 193–217. https://doi.org/10.1016/s0169-555x(00)00036-2

Soar, P. J., & Thorne, C. R. (2001). *Channel restoration design for meandering rivers*. Vicksburg, MS: Engineer Research And Development Center. 10.21236/ADA397049

Solari, L., Van Oorschot, M., Belletti, B., Hendriks, D., Rinaldi, M., & Vargas-Luna, A. (2016). Advances on modelling riparian vegetation-hydromorphology interactions. *River Research and Applications*, *32*, 164–178. https://doi.org/10.1002/rra.2910

Stanton, J., Marek, J., Hall, L., Kus, B., Alvarado, A., Orr, B., et al. (2019). Recovery planning in a dynamic system: Integrating uncertainty into a decision support tool for an endangered songbird. *Ecology and Society*, *24*. https://doi.org/10.5751/es-11169-240411

Stillwater Sciences. (2011). *Assessment of geomorphic processes for the upper Santa Clara River watershed, Los Angeles county, California*. Berkeley: California for Ventura County Watershed Protection District, Los Angeles County Department of Public Works, and the U.S. Army Corps of Engineers–L.A. District. Final report. Prepared by Stillwater Sciences.

Stillwater Sciences & URS Corporation. (2007). *Riparian vegetation mapping and preliminary classification for the lower Santa Clara River and major tributaries, Ventura County, California*. Berkeley, California: Prepared by Stillwater Sciences and URS Corporation for the California State Coastal Conservancy and the Santa Clara River Trustee Council.

Stover, J. E., Keller, E. A., Dudley, T. L., & Langendoen, E. J. (2018). Fluvial geomorphology, root distribution, and tensile strength of the invasive giant reed, Arundo donax and its role on stream bank stability in the Santa Clara River, southern California. *Geosciences*, *8*, 304. https://doi.org/10.3390/geosciences8080304

Tal, M., & Paola, C. (2010). Effects of vegetation on channel morphodynamics: Results and insights from laboratory experiments. *Earth Surface Processes and Landforms*, *35*, 1014–1028. https://doi.org/10.1002/esp.1908

Van Oorschot, M., Kleinhans, M. G., Geerling, G. W., Egger, G., Leuven, R., & Middelkoop, H. (2017). Modeling invasive alien plant species in river systems: Interaction with native ecosystem engineers and effects on hydro-morphodynamic processes. *Water Resources Research*, *53*, 6945–6969. https://doi.org/10.1002/2017wr020854

Warrick, J. A., & Mertes, L. A. (2009). Sediment yield from the tectonically active semiarid western transverse ranges of California. *Geological Society of America Bulletin*, *121*, 1054–1070. https://doi.org/10.1130/b26452.1

Warrick, J. A., & Rubin, D. M. (2007). Suspended-sediment rating curve response to urbanization and wildfire, Santa Ana River, California. *Journal of Geophysical Research*, *112*. https://doi.org/10.1029/2006jf000662

Wijte, A. H., Mizutani, T., Motamed, E. R., Merryfield, M. L., Miller, D. E., & Alexander, D. E. (2005). Temperature and endogenous factors cause seasonal patterns in rooting by stem fragments of the invasive giant reed, Arundo donax (Poaceae). *International Journal of Plant Sciences*, *166*, 507–517. https://doi.org/10.1086/428915

Williams, R. P. (1979). *Sediment discharge in the Santa Clara River basin, Ventura and Los Angeles counties, California* (p. 51). US Geological Survey, Water Resources Division. https://doi.org/10.3133/wri7978